Surface Plasmon Resonance Monitoring of Mono-Rhamnolipid Interaction with Phospholipid-Based Liposomes

Meryem Belkilani, Maryam Shokouhi, Carole Farre, Yves Chevalier, Sylvain Minot, François Bessueille, Adnane Abdelghani, Nicole Jaffrezic-Renault, Carole Chaix

SPR monitoring of mono-rhamnolipid interaction with phospholipid-based liposomes

Meryem Belkilani,[†] [‡] [§] Maryam Shokouhi[⊥] Carole Farre,[†] Yves Chevalier,[#] Sylvain Minot,[†] François Bessueille,[†] Adnane Abdelghani,[§] Nicole Jaffrezic-Renault,[†] Carole Chaix[†]*

[†]*University of Lyon, CNRS, Claude Bernard Lyon 1 University, Institute of Analytical Sciences, 5 rue de la Doua, F-69100 Villeurbanne, France.* [‡]*University of Tunis, ENSIT, Avenue Taha Hussein, Montfleury, 1008 Tunis, Tunisia.* [§]University *of Carthage, INSAT, Research Unit of Nanobiotechnology and Valorisation of Medicinal Plants,* 1080 Charguia Cedex, Tunisia. [⊥]*University of Isfahan, Department of chemistry, Isfahan 81746-73441, Iran.* [#]*University of Lyon, CNRS, Claude Bernard Lyon1 University, LAGEPP, 43 Bd 11 Novembre, F-69622 Villeurbanne, France.*

[*] Corresponding authors: carole.chaix-bauvais@univ-lyon1.fr

KEYWORDS. Multi-parametric surface plasmon resonance, Liposome, Mono-rhamnolipid, Phospholipid.

ABSTRACT

The interactions of mono-rhamnolipids (mono-RLs) with model membranes were investigated through a biomimetic approach using phospholipid-based liposomes immobilized on a gold substrate and also by the multi-parametric surface plasmon resonance (MP-SPR) technique. Biotinylated liposomes were bound onto a SPR gold chip surface coated with a streptavidin layer. The resulting MP-SPR signal proved the efficient binding of the liposomes. The thickness of the liposome layer calculated by modeling the MP-SPR signal was about 80 nm, which matched the average diameter of the liposomes. The mono-RL binding to the film of the phospholipid liposomes was monitored by SPR and the morphological changes of the liposome layer were assessed by modeling the SPR signal. We demonstrated the capacity of the MP-SPR technique to characterize the different steps of the liposome architecture evolution, i.e. from a monolayer of phospholipid liposomes to a single phospholipid bilayer induced by the interaction with mono-RLs. Further washing treatment with Triton X-100 detergent left a monolayer of phospholipid on the surface. As a possible practical application, our method based on a biomimetic membrane coupled to a SPR measurement proved to be a robust and sensitive analytical tool for the detection of mono-RLs with a limit of detection of 2 μg mL^{-1}.

INTRODUCTION

Rhamnolipids are secondary metabolites naturally produced by the bacteria *Pseudomonas aeruginosa*, with biosurfactant properties. They belong to the group of surface-active glycolipids

and consist of a glycone part composed of one or two rhamnose moieties connected via an α-1,2-glycosidic linkage and a glycone part consisting of two alkyl chains. They are produced as a mixture of mainly α-L-rhamnopyranosyl-β-hydroxydecanoyl-β-hydroxydecanoate and 2-O-α-L-rhamnopyranosyl-α-L-rhamnopyranosyl-β-hydroxydecanoyl-β-hydroxydecanoate called mono- and di-rhamnolipid respectively. These two compounds are the dominant components in the naturally produced mixture. They constitute the virulence factor of *P. aeruginosa* and they cause chronic respiratory infections in cystic fibrosis patients and immunocompromised individuals. It has been shown on *in vitro*-reconstituted human respiratory epithelium that incorporating rhamnolipids in a host cell membrane decreases transepithelial resistance for concentrations higher than 50 μg mL.[1] Rhamnolipids are incorporated within the apical membranes of epithelial cells and later within their basolateral membranes. The permeability of epithelia to bacteria is then increased. As biosurfactants, rhamnolipids are used in detergents, food and cosmetic products, as those compounds have low toxicity and a weak ecological impact.[2]

Because of complexity due to the numerous biological activities of rhamnolipids, interactions of rhamnolipids with cell membranes still deserve detailed investigations. Biomimetic membrane models facilitate the understanding of complex biological membrane behaviors. Those composed of lecithins, the main phospholipids of many living cells, are structured as bilayers that may be dispersed in water as liposomes or vesicles. These types of vesicles, encapsulating redox or fluorescent probes have been used for the detection of various microorganisms through their metabolites. [3-4] Calorimetric studies have shown that di-RLs bind to mono-unsaturated phospholipid 1-palmitoyl-2-oleoyl-glycero-3-phosphocholine (POPC) vesicles, rupture the bilayers and cause leakage from the inner aqueous medium at RL/lipid ratios higher than one, this effect being reduced in the presence of cholesterol.[5] A FTIR study showed a direct interaction

between the phosphate groups of 1-palmitoyl-2-linoleoyl-*sn*-glycero-3-phosphocholine (PLPC) and the polar heads of rhamnolipids, then altering the organization of polar headgroups of the phospholipids. These interactions were confirmed by molecular dynamics simulations of these membrane models in the presence of rhamnolipids.[6] Owing to their two rhamnose units in their polar headgroup, di-RLs are more hydrophilic surfactants than mono-RLs.[7] Thus, di-RLs self-assemble as small micelles which grow as the concentration increases. Conversely, the less hydrophilic mono-RLs form large micelles and vesicles in aqueous solution. On that basis, mono-RLs are more prone to mix with phospholipids and to be incorporated into liposome bilayers.

Surface plasmon resonance (SPR) is a suitable label-free technique for the study of interactions between species bound to the SPR chip surface and their partners in solution. The Kretschmann configuration enables measurements avoiding interference from the surrounding liquid medium because incident light does not pass through this medium. Moreover, SPR measurements performed with two different wavelengths of incident light allow a unique pair of values of the thickness and refractive index of the films deposited on the gold surface to be determined.[8-9]

In the past few years, a number of studies have investigated the deposition of either planar mono- or bi-lipidic layers, or liposomes on gold substrates by SPR. [10-17]. These membrane biomimicking systems have been applied to the study of the interactions with different molecules such as catechol,[18] drugs,[19] peptides,[20-21] , proteins,[22-24] or toxins.[25] To our knowledge, the SPR technique has not been used so far for studying the interactions of rhamnolipids with phospholipid layers or liposomes. The objective of this work was to assess the mechanism of interaction of RLs with a biomimetic membrane formed by a monolayer of liposomes. First, the immobilization of phosphatidylcholine-based liposomes on functionalized gold SPR chips was monitored. The thickness and refractive index of the different layers were deduced by modeling the SPR signals at

two wavelengths. Then, RL solutions of different concentrations were flowed on the liposome layer and SPR signals (sensorgrams) were recorded. A solution rich in mono-RLs was preferred for this study because mono-RLs are presumed to bind more strongly to phospholipid bilayers than di-RLs .[7, 26] A RL mixture rich in mono-RLs may destructure phospholipid liposomes with better efficacy. The change of the morphology of the liposome layer was then described, based on modeling of the SPR signal.

MATERIALS AND METHODS

Chemicals. Hydrogenated soybean phosphatidylcholine (HSPC) was purchased from Lipoid company, 1,2-distearoyl-*sn*-glycero-3-phosphoethanolamine-N-[biotinyl(polyethylene glycol)-2000] (DSPE-PEG), cholesterol (99 %), 11-mercaptoundecanoic acid (MUA), 11-amino-1-undecanethiol hydrochloride, 1-dodecanethiol, streptavidin, 1-(3-dimethylaminopropyl)-3-ethylcarbodiimide (EDC), N-hydroxysuccinimide (NHS), ethanolamine, mono-rhamnolipid (mono-RL) R95Md (95 % pure rhamnolipids, mono-rhamnolipid dominant) produced by AGAE Technologies LLC (USA), Triton X-100, NaCl were provided by Sigma-Aldrich. Chloroform (99.8 %) was bought from Fisher Chemical. Diethyl ether was purchased from Carlo Erba. Methanol was ordered from VWR company. 2-(N-morpholino) ethanesulfonic acid (MES) was purchased from Dominique Dutcher company. Ultrapure water was obtained using a Milli-Q system (resistivity 18.2 MΩ cm).

Preparation of biotinylated liposomes. Biotinylated liposomes were prepared for immediate use according to the “thin layer rehydration” technique and a slightly modified protocol from that developed by Zhao *et al*.[27] HSPC, DSPE-PEG and cholesterol (610.8 mg, 9.8 mg and 200 mg

respectively) were dissolved in 75 mL of a mixed organic solvent: chloroform, diethyl ether and methanol (5.75 : 5.75 : 1 V/V). Biotinylated phospholipids represent 1.5% (W/W) of the total phospholipids used in this protocol. Organic solvents were then evaporated under a vacuum of −0.05 MPa in a water bath at 50 °C for 3 hrs using a rotary evaporator (Buchi Rotavapor R-114 with Heating Waterbath B-480 & Glassware- Acomertial). The thin transparent layer in the round bottom flask was hydrated with water at 60 °C by rotating the container for 1 hr, until the thin layer was completely dispersed in water and a milky suspension solution was obtained. In order to obtain a homogeneous mixture and to reduce the average size of the liposomes, the solution was sonicated for 20 min with a UP400S – Powerful Sonication of Larger Samples (Hielscher – Ultrasound Technology company) at 60 kHz in an ice bath. The liposome solution was stored at room temperature until further use.

Physicochemical characterization of liposomes. Hydrodynamic diameter measurements were performed at 25 °C by Dynamic Light Scattering (DLS) with a Zetasizer NanoZS instrument (Malvern Panalytical, Palaiseau, France) operating in backscatter mode at an angle of 173°. A disposable polystyrene cuvette was filled with 3 mL of a diluted liposome suspension (1:10) in a 0.15 M NaCl solution and measurements in triplicate were started after an equilibration time of 60 s. Results are based on intensity distribution calculation; they are given as an average hydrodynamic diameter ± standard deviation (*SD*) with a polydispersity index (*PdI*).

The surface charge of the liposomes was determined by ζ-potential measurements using a NanoZS Zetasizer instrument (Malvern Panalytical). The measurements were carried out in folded capillary cells DTS 1070 (Malvern Instruments), which were filled with 800 µL of a diluted liposome suspension (1:10) in 0.15 M NaCl solution and equilibrated at 25 °C for 60 s.

The refractive index of the prepared liposome suspensions was determined using an PAL-1 ATAGO refractometer.

Cryo-TEM observations were performed on diluted dispersions of purified liposomes. A drop of dispersion was cast onto a 300 mesh holey carbon film (Quantifoil R2/1) and quench-frozen in liquid ethane using a cryo-plunge workstation (LPS, University of Paris-Saclay, France). The specimens were then mounted on a precooled Gatan 626 sample holder, transferred into the microscope (Phillips CM120) and observed at an accelerating voltage of 120 kV.

Functionalization procedure of the SPR gold chips. SPR gold chips were obtained from BioNavis (BioNavis Ltd., Ylöjärvi, Finland). They were typically 20 mm long, 12 mm wide and 0.55 mm thick, consisting of a (∼50 nm) Au layer on a (∼3 nm) Cr adhesive layer on a glass slide that has a refractive index of 1.52020 and 1.51620 at 670 nm and 785 nm respectively. The gold surface roughness was 1.53 nm. It was measured by Atomic Force Microscopy (AFM) operating in tapping mode (Agilent M5500 Picoplus®, Agilent Technologies, Palo Alto, CA, USA), and corresponds to the root mean square roughness (RMS) for an image of 2.5 × 2.5 μm in size.

The SPR gold chips were used as substrates after the following procedures:

- Any potential contaminants were removed by microwave induced plasma generated by a microwave plasma reactor (UHP-MW-PC, Diener electronic company, Stuttgard, Germany). The operating pressure was generated by a dry-vacuum pump. We used two successive steps for plasma treatment. The first step was cleaning using dioxygen at a pressure of 0.7 mbar for 3 min with a power of 180 W dm^3. To ensure the grafting of the thiols onto the metallic surface by avoiding the potential risk of oxidation, the second step was a reducing plasma treatment. We achieved this second step using dihydrogen at a pressure of 1 mbar for 5 min with a power of 126 W dm^3. Then, the slides were sonicated for 5 min in acetone and next in ultrapure water.

- To form a dense self-assembled monolayer (SAM) on the gold surface, the Au substrates were dried under a nitrogen flow and immediately immersed in a 1 mM ethanolic solution of 11-mercaptoundecanoic acid (MUA) (acidic SAM) or of 11-amino-1-undecanethiol hydrochloride (amino SAM) or of 1-dodecanethiol (alkyl SAM) for a minimum duration of 20 hrs at 4 °C. The chips were then rinsed with ethanol and dried under a gentle nitrogen flow. SPR gold chips functionalized with the different SAMs were preserved in an ultrapure water bath and used directly for the liposome immobilization.

- To develop the streptavidine SPR chip, the gold surface was cleaned by plasma treatment as described above and immersed in an ethanolic solution of 11-mercaptoundecanoic acid (MUA, 1 mM) for 20 hrs at 4 °C.[28] Then the chip was rinsed with ethanol and dried under a gentle flow of nitrogen. The MUA SPR gold chip was incubated in 100 µL of a mixture of 0.2 M EDC and 0.05 M NHS in MES buffer (5 mM MES, pH 5) for 2 hrs at room temperature. The activated surfaces were washed in 1 mL of MES buffer and then incubated in 100 µL of a streptavidin solution (1 mg mL^{-1}) in PBS buffer (0.1M NaH_2PO_4, 0.1 M Na_2HPO_4, 0.15 M NaCl, pH 7) for 12 hrs at room temperature. Afterwards, SPR chip surfaces were rinsed with 1 mL of MES buffer, incubated in 2 mL of 10 mM ethanolamine aqueous solution for 10 min to block the residual activated acid functions and remove all the physisorbed streptavidin, and rinsed again in 1 mL of MES buffer. All functionalization steps were monitored by SPR under a 0.15 M NaCl solution flow.

Multi-parametric surface plasmon resonance (MP-SPR). Dual wavelength surface plasmon resonance measurements were performed with a MP-SPR Navi™ 200 OTSO (BioNavis Ltd., Ylöjärvi, Finland) instrument at ambient temperature. The setup was equipped with a two laser source excitation providing 670 nm and 785 nm incident wavelengths, two independent flow channels, inlet tubing and an outlet for waste tubing. The measurements in both flow channels were

carried out in parallel with the incident lights of 670 nm and 785 nm. The intensity of the reflected light was measured at a resonant angle between 40 ° and 78 °.

During the SPR measurements on the gold chips functionalized with amino SAM, alkyl SAM, acidic SAM and streptavidin, a continuous flow (50 µL min^{-1}) of a 0.15 M NaCl solution was firstly injected for approximately 10 min until the SPR sensorgram signal was stabilized. After stabilization of the signal intensity, different concentrations of liposomes (1×10^{11} – 5×10^{12} liposomes mL^{-1}) in a 0.15 M NaCl solution were injected onto the SPR gold chips in both flow channels for 4 min at a flow rate of 50 µL min^{-1}, in order to evaluate which type of functionalization insures a dense layer of liposomes.

Liposome–Rhamnolipid interaction analysis. The MP-SPR measuring instrument was used for monitoring interactions between mono-RLs and liposomes. The mono-RL solutions were prepared in 0.15 M NaCl, in a range of concentrations from 2 to 100 µg mL^{-1}, and then injected onto the liposome layer. 2 µg mL^{-1}, 5 µg mL^{-1}, 10 µg mL^{-1} and 20 µg mL^{-1} mono-RL solutions were injected at a flow rate of 12 µL min^{-1} for 15 min, while the concentrations of 50 µg mL^{-1}, 80 µg mL^{-1} and 100 µg mL^{-1}were injected at a flow rate of 50 µL min^{-1} for 4 min. Each injection was followed by a 4 min washing step with 0.15 M NaCl solution at 50 µL min^{-1} until the signal was stabilized. This protocol provided an optimal variation of the SPR signal during the sensorgram. Finally, 1 mL of Triton X-100 (1 %) in a 0.15 M NaCl solution was injected into both channels for 4 min. Each experimental procedure was reproduced twice.

MP-SPR biophysical analysis. The theoretical simulation of the multilayer system and the determination of the optical parameters of the different layers were performed by the SPR Navi LayerSolver v. 1.2.1 (BioNavis Ltd., Ylöjärvi, Finland) software, which is supplied as associated software with the MP-SPR instrument. The LayerSolver software uses the well-known Fresnel

equation formalism for calculations.[29-30] The multi-layer calculation method is based on a numerical layer by layer iteration and allows for multiple SPR spectra processing, and a stepwise approach for calculations. A theoretical description for the resonance condition can be obtained by solving Maxwell's equations for a multilayer optical system.[29] The software was used to simultaneously determine the thickness and refractive index giving the best fit of the theoretical calculation to the full SPR angular spectra measured at both laser wavelengths at the same time, and at the same point.[8, 29] The two-wavelength method combined with angular scanning over a wide range of incidence angles has proven to be particularly efficient to retrieve the layer thickness and refractive index values of the thin biomolecular layers.[9, 31-32]

The schematic representation of the multilayer system is presented in Figure 1. Layers 0 to 4 of the SPR gold chip are the glass substrate, the chromium-gold layer, the SAM, the streptavidin layer and the liposome layer, respectively. It is worth noting that the MP-SPR Fresnel's reflection coefficient is based on an independent layer model structure. Each layer is characterized by its thickness (d) and its complex refractive index ($\tilde{n}$)[33] calculated with equation 1:

$$\tilde{n} = n + ik \quad (1)$$

where n is the real part of the refractive index that corresponds to the refraction of light and k is the imaginary part corresponding to the extinction or absorption of light by the material.

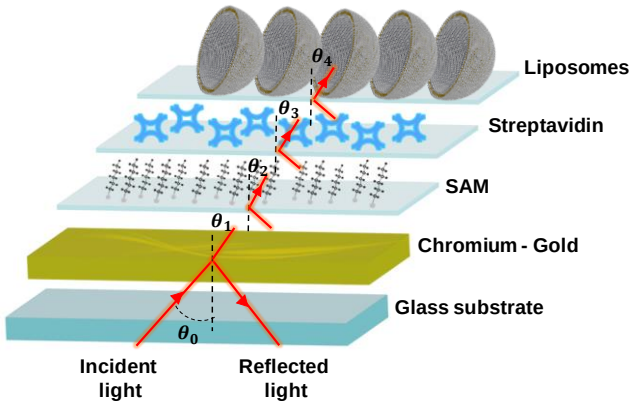

Figure 1. Schematic representation of the multilayer system of the SPR gold chip.

Since the SPR full angle spectra at both wavelengths are measured at the same location, the layer thickness should be the same for both wavelengths. The thickness values were therefore defined as global variables for both wavelengths. The complex refractive index was considered as an independent variable for the metal layer modeling ($k \neq 0$) and as a linearly dependent variable between the two used wavelengths for the other organic layers that do not absorb light ($k = 0$). The refractive index of the layer for the second wavelength, $n_{\lambda 2}$, can be calculated using equation 2 [30].

$$n_{\lambda 2} = n_{\lambda 1} + \frac{\mathrm{d}n}{\mathrm{d}\lambda} \times (\lambda 2 - \lambda 1) \quad (2)$$

where $n_{\lambda 1}$ is the refractive index for wavelength 1, and $\frac{\mathrm{d}n}{\mathrm{d}\lambda}$ is the linear dispersion coefficient relative to wavelength-change.

The optical input parameters of chromium and gold layers are taken from MP-SPR Navi LayerSolver User Manual as follows: for the chromium adhesion layer $\tilde{n}_{670} = 3.52950 + i4.26830$ and $\tilde{n}_{785} = 3.97290 + i4.18950$; for the gold layer, $\tilde{n}_{670} = 0.17410 + i3.61230$ and $\tilde{n}_{785} = 0.18360 + i4.58710$. The other parameters were determined by fitting to the experimental data.

The changes of the thickness and refractive index at the surface of the SPR gold chips induce a shift of the SPR angular peak minimum (θ_{SPR}). Thus, based on Feijter's formula,[34] the surface mass density (Γ) of an adsorbed liposome layer can be calculated using equation 3, considering the SPR measured parameters of the layer.

$$\Gamma = \frac{d_L \times (n_L - n_b)}{\mathrm{d}n/\mathrm{d}c} \quad (3)$$

where d_L, n_L are the thickness and refractive index respectively of the corresponding layer L, n_b is the refractive index of the NaCl solution at each wavelength, and dn/dc is the refractive index increment of the dispersion of liposomes. An accurate determination of dn/dc is necessary to precisely quantify the surface mass densities (Γ) of liposomes. dn/dc was determined experimentally from the slope of the linear variation of the refractive index as a function of liposome concentrations (C_l). The obtained value, dn/dc ≈ 0.134 $cm^3\ g^{-1}$, is comparable to values reported in the literature (dn/dc $_{lipid}$ ≈ 0.135 $cm^3\ g^{-1}$).[35-36]

RESULTS AND DISCUSSION

Biotinylated liposome characterization. The liposomes were characterized with respect to their size and surface charge. The hydrodynamic diameter of liposomes determined by DLS (Table 1) was around 76 nm, with a polydispersity index (*PdI*) of 0.16. It can be noted that the liposome size was less than half of both wavelengths of the MP-SPR device, so that the evanescent wave could penetrate the full liposome layer. In addition, the surface potential of the liposomes was measured on the basis of their electrophoretic mobility. The Zeta potential value was approximately −10.8 mV. The negative surface of the liposomes, due to the phosphate groups of the phospholipids, induces an electrostatic repulsion between them, preventing their aggregation and providing high colloidal stability. Several measurements of these parameters over time confirmed

the stability of the liposome suspensions over a period of 6 months. Furthermore, the liposome suspension was carefully controlled before each SPR experiment.

Table 1. Properties of the biotinylated liposomes; the hydrodynamic diameter and zeta potential are given as mean values ± standard deviation of three independent measurements.

Diameter (nm)	***PdI*[a]**	**Zeta potential (mV)**	***C*p [b] (mmol L^{-1})**	***C*l [c] (lipo mL^{-1})**	***RI*[d]**
76 ± 7.5	0.16	−10.8 ± 0.6	30	2.5×10^{14}	1.34

[a] Polydispersity index, [b] Concentration of phospholipids, [c] Concentration of liposomes, [d] Refractive index

The liposome concentration C_l is obtained by dividing the total number of liposomes N_{lipo} (calculated according to equation S1 in Supporting Information) by the volume of the suspension (V = 25 mL), resulting in 2.5×10^{14} lipo mL^{-1}.

Cryo-TEM observation confirmed the size of the synthetized liposomes. As shown in Figure 2a, the liposomes appeared as perfectly spherical and unilamellar nanovesicles. Figure 2b presents the size distribution of liposomes, estimated with ImageJ software. The mean diameter of the liposomes was 69 nm with a standard deviation of 10 nm.

Satisfactory agreement is noticed between the two size distributions derived from TEM image analysis and DLS measurements. The measurement of the hydrodynamic diameter of liposomes by DLS in solution takes into account a layer of hydration around the liposomes, which leads to a difference of around 10% with the diameter measured by Cryo TEM.

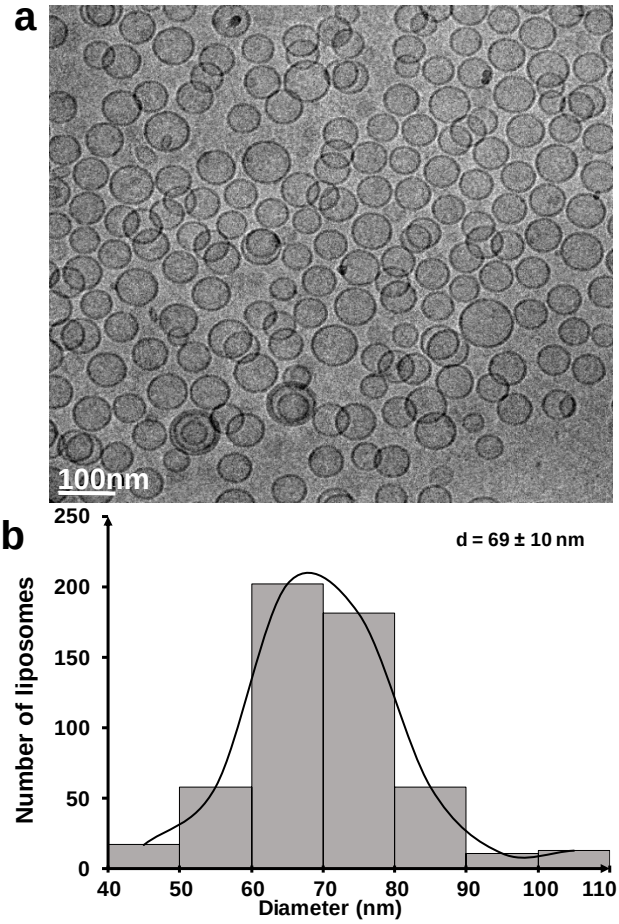

Figure 2. (a) TEM image and (b) diameter histogram of a diluted dispersion of biotinylated liposomes.

SPR monitoring of liposome immobilization on modified surfaces. A comparative study of the interaction of biotinylated liposomes with several SAM-functionalized gold SPR chips was performed so as to select a SAM binding a dense layer of immobilized liposomes. For this purpose, the gold surface underwent different functionalizations. After thorough cleaning of the gold SPR chip, self-assembled monolayers (SAMs) of long-chain alkanethiols with varying terminal groups (–COOH, $–NH_2$, and $–CH_3$) were formed on gold chips after 20 hrs reaction. A fourth gold chip was functionalized by a streptavidin layer by a two-step protocol: A closely packed 11-

mercaptoundecanoic acid layer was first elaborated on the gold surface. Then, the acidic function was activated using EDC/NHS chemistry in order to covalently graft the streptavidin to the SPR chip surface.

During the measurement and to ensure the accuracy of the changes in the measured optical parameters, a calibration step of the SPR device with 0.15 M NaCl solution was made. Next, biotinylated liposome dispersions at concentrations between 1×10^{11} and 5×10^{12} lipo mL^{-1} were injected and flowed at 50 µL min^{-1} for an interaction time of 4 min with the functionalized chips. This was followed by a 4 min washing step in 0.15 M NaCl to remove unbound liposomes. The variation in the θ_{SPR} position ensuing from the variation of the refractive index as a function of different liposome concentrations (C_l) was compared for the four different functionalized surfaces (Figure 3).

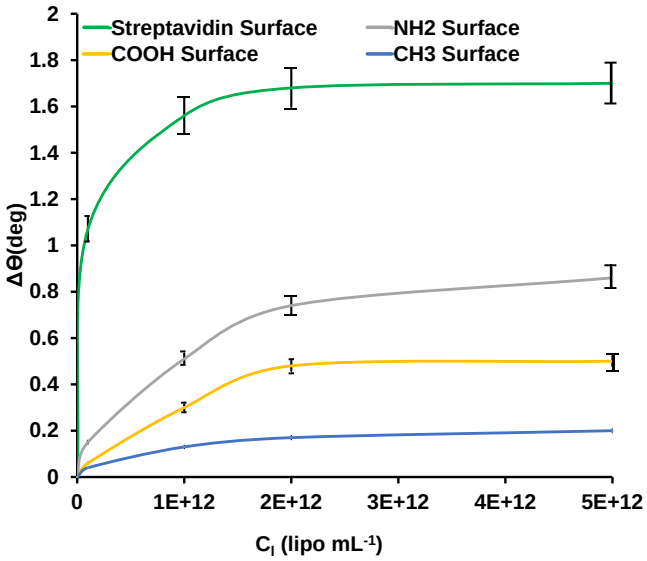

Figure 3. Angular shifts of the resonance peak ($\Delta\Theta_{SPR}$) in SPR measurements at 670 nm versus liposome solution injection at different concentrations (C_l). The interactions of biotinylated liposome solutions were studied on –COOH (11-mercaptoundecanoic acid), –NH_2 (11-amino-1-undecanethiol), –CH_3 (1-dodecanethiol) and streptavidin modified SPR gold surfaces.

After calibration of the device, the SPR measurement of the functionalized gold surface was performed before the injection of the liposomes. Streptavidin deposition on the 11-mercaptoundecanoic acid layer resulted in a 0.4 ° variation of the θ_{SPR}, whereas the deposition of the different self-assembled monolayers on gold led to a signal variation of approximately 0.2 °. As shown in Figure 3, liposomes bound strongly to the streptavidin-functionalized surface, resulting in a θ_{SPR} increase of 1.7 ° under injection of 5×10^{12} lipo mL^{-1}. By modifying the gold surface with an amino terminated layer, the angular shift was substantial (0.86 °) but remained weak compared to the one obtained during the liposome binding on the streptavidin chip. The binding interaction on the amino terminated layer was mainly driven by electrostatic interaction.

In the case of the 11-mercaptoundecanoic acid layer, a low angular shift of 0.48 ° was obtained, that reflected a clear blocking effect due to electrostatic repulsion. However, this binding was even stronger than for the hydrophobic SAM (1-dodecanethiol) which prevented hydrophilic liposomes from binding, resulting in a small angle variation (0.2 °). Thus, the order of the angle variation $\Delta\theta$ following the liposome immobilization on SAM surfaces was as follows: $\Delta\theta_{\text{NH2 surface}} > \Delta\theta_{\text{COOH surface}} > \Delta\theta_{\text{CH3 surface}}$. These results are in good agreement with experimental results reported by Fenzl *et al.*[15] for the interaction of negatively charged liposomes (DPPC/DPPG/cholesterol liposomes with a Zeta potential of -34 mV and DPPC/DPPG/N-glutaryl DPPE/cholesterol with a zeta potential of -47 mV) with varying charge and hydrophilicity surfaces. They noted the same order of variation for refractive index values, i.e. $\Delta n_{\text{NH2 surface}} > \Delta n_{\text{COOH surface}} > \Delta n_{\text{CH3 surface}}$, when injecting a 453 pM (~2.5×10^{12} lipo mL^{-1}) concentration of liposomes on gold surfaces modified by 11-mercaptoundecyl amine hydrochloride, 11-mercaptoundecanoic acid (MUA) and 1-mercaptoundecane SAMs. In our case, the liposome surface was less anionic, and had PEG moieties that can play a role in the interactions. We assume that the attractive interaction between the anionic liposomes and the cationic amino surface was not sufficiently effective to obtain a homogeneous layer of liposomes compared with streptavine-functionalized gold substrate.

The efficiency of washing with the Triton X-100 detergent was assessed at this stage. After immobilization of liposomes and signal stabilization in NaCl solution, Triton X-100 (1 %) was injected on the surface of each SPR chip leading to phospholipid release. Thus, the success of liposome binding to the streptavidin-functionalized surface was indirectly demonstrated by the Triton treatment. As expected, a significant drop of the SPR signal down to the baseline was observed for the liposomes immobilized on SAM-functionalized surfaces after the injection of Triton X-100, whatever the quantity of immobilized liposomes (see Figure S1 in Supporting

Information). Further details on the calculation of residual liposome masses after Triton treatment will be discussed later in the text. The streptavidin modified SPR gold surface was preferred for liposome coating, on the basis of its strong affinity[37] leading to efficient loading and good layer stability.

SPR gold chip layers: formation and modeling. Figure 4a shows the time-resolved sensorgram obtained after saturation by 1×10^{14} lipo mL^{-1} of biotinylated liposomes on the streptavidin layer. The variation of θ_{SPR} reached about 1.7 ° and this value remained constant during the washing step with 0.15 M NaCl solution. This value obtained in a single injection is the same as that following cumulative injections of increasing concentrations of liposomes up to 5×10^{12} lipo mL^{-1} as presented in Figure 3. Both experiments show the saturation of the SPR gold surface at this coverage.

Figure 4b (light source at 670 nm) and Figure S2 (light source at 785 nm, see Supporting Information) present the SPR full angle scans recorded from 55 to 77 ° and 60 to 72°, respectively. The angular shift of the SPR confirmed the success of the successive functionalizations of the gold surface. Indeed, the θ_{SPR} recorded for the metal (yellow trace, θ_1 = 68.63 °) shifted to the right when the 11-mercaptoundecanoic acid layer was deposited on the surface (red trace, θ_2 = 68.89 °), and the SPR peak subsequently moved farther to the right when streptavidin was adsorbed (green trace, θ_3 = 69.41 °). Interestingly, the SPR peak recorded after the liposome immobilization on streptavidin was the largest of all (blue trace, θ_4 = 71.4 °). In addition, we noted the absence of any peak in the vicinity of the total internal reflection (TIR) angle where a second peak is likely to appear when the thickness of the liposome layer exceeds the penetration depth of the evanescent

SPR field. Indeed, it was reported in the literature that this exotic optical behavior of the full SPR angular spectrum was due to the formation of a waveguide on the SPR gold chip.[38]

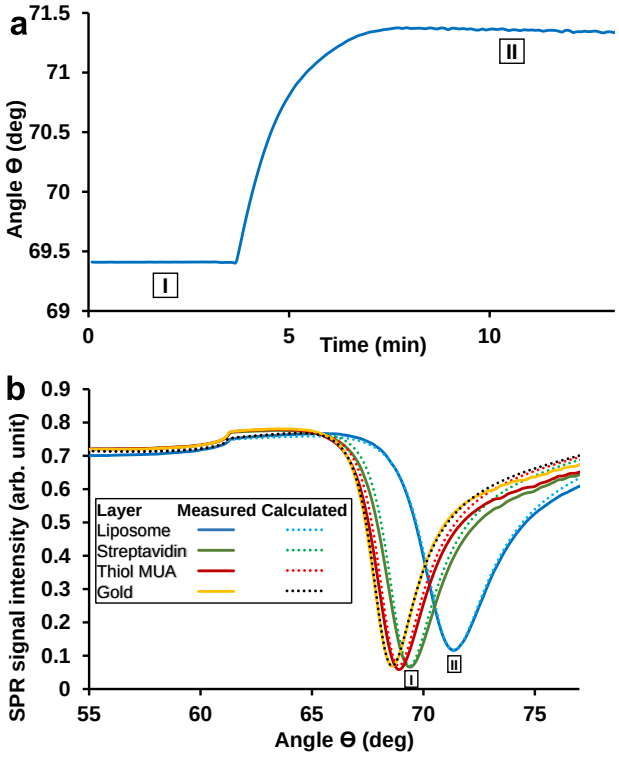

Figure 4. (a) SPR sensorgram of the immobilization of 1×10^{14} lipo mL^{-1} liposomes on a streptavidin functionalized SPR chip, with light source at 670 nm. (b) SPR full angle scans of the SPR gold chip at the different steps of the functionalization: gold layer (yellow line), 11-mercaptoundecanoic acid layer (red line), streptavidin layer (green line) and liposome layer (blue line), with corresponding fits (dashed lines) from LayerSolver modeling of individual SPR chip layers using the full SPR angular spectra measured at 670 nm wavelength. Roman numerals (I and II) show the correspondence of events in the sensorgram (a) and the SPR angle scans (b).

To confirm the formation of the layers and quantify the adsorption, a dual wavelength analysis for the determination of thicknesses (d) and refractive indexes ($\tilde{n}$) was performed with the layer resolution software LayerSolver. These parameters were independently calculated after several measurements and obtained when the upper and lower limits of the layer thicknesses and refractive indexes were fixed. The d and $\tilde{n}$ values were calculated using a consistent set of initial values throughout the modeling in order to evaluate the dynamic behavior of the modeled systems and the sensitivity of the differential equations to the initial conditions provided as inputs to LayerSolver. The parameters (d and n) coming from the liposome layer modeling as well as the other layers are reported in Table 2. The results for each individual measurement are shown in Table S1 (Supporting Information).

Table 2: Thickness (d) and refractive index (n) of the different layers of the SPR chip, obtained by SPR LayerSolver simulation. The calculated values represent the average (± standard deviation) of three independently repeated measurements.

Layer	d (nm)	n_{670}	n_{785}
Glass	Infinite (starting layer)	n = 1.52020	n = 1.51620
Chromium	1.6 ± 0.06	n = 3.51127 ± 0.02050	n = 4.04615 ± 0.17135
Gold	54.98 ± 0.02	n = 0.19612 ± 0.00016	n = 0.19548 ± 0.00477
Thiol MUA	1.50 ± 0.08	n = 1.43897 ± 0.01385	n = 1.42702 ± 0.01378
Streptavidin	2.71 ± 0.31	n = 1.41646 ± 0.01102	n = 1.41416 ± 0.01102
Liposome	79.61 ± 6.74	n = 1.35270 ± 0.00122	n = 1.35102 ± 0.00126
NaCl solution	Infinite (ending layer)	n =1.33216	n =1.32966

All simulations were performed with an electrolyte solution of 0.15 M NaCl and under the excitation of incident light at 670 nm and 785 nm. The simulation started with the determination

of the optimized optical properties for the chromium adhesion layer 'Cr' and the gold layer 'Au' by modeling a full SPR angle spectrum of a cleaned SPR gold chip. Then, the optical properties of the SPR chip were maintained as fixed and used as the starting point to determine the optical properties of the different deposited layers.

For the determination of the MUA layer parameters, the Fresnel equations for a system of five layers (Prism (glass)/Cr/Au/MUA films/NaCl) were used. MUA forms, on average, a thin layer on the surface of the SPR gold chip, with a thickness of 1.5 nm and a refractive index of 1.44 at 670 nm. These results are in good agreement with the numerical analysis results of Damos *et al*. who calculated a film thickness of about 1.55 nm with a dielectric constant of $\varepsilon = n^2 = 2.1$ at 670 nm for the adsorption of MUA on the gold surface. [39] Adding the parameters found for the MUA layer to the calculating system, a thickness of 2.7 nm was determined for the streptavidin layer (spectrum I) with a refractive index of 1.42 at 670 nm. Our theoretical simulation reproduced well the modeling results reported by Schmidt *et al*. [40] and Dolci *et al.* [41] for a streptavidin layer. They measured 2.8 nm and 3 nm thicknesses together with 1.45 and 1.5 refractive indexes respectively.

The SPR spectrum (II, Figure 4b) taken after signal stabilization corresponds to the liposome layer. Liposomes immobilized on the streptavidin functionalized chip form a layer of about 80 nm average thickness. The calculated refractive indexes at both wavelengths were $n_{670} = 1.35270$ and $n_{785} = 1.35102$. The layer thickness corresponded to the liposome diameter measured by DLS and TEM and further adsorption did not occur when the liposome concentration in the solution was increased again. This strongly suggests that liposomes adsorb as a monolayer. The difference of the theoretical thickness value compared to the hydrodynamic diameter measured in bulk can be

attributed to morphological changes in the liposome shape due to the interactions with the functionalized gold chip surface and to the shear stress due to the buffer flow.

The liposome addition induced a shift of the SPR curve towards higher incidence angles which became wider due to the increased thickness of the adsorbed layer on the surface.

In most biomolecular interaction studies, layer thicknesses are lower than the penetration depth of the evanescent field. This is so in the present case; the evanescent wave of the SPR can penetrate the whole liposome layer adsorbed on the SPR chip surface because the liposome average diameter is less than half that of the wavelengths (670 and 785 nm) of the MP-SPR device.[14, 33] The adsorption as a dense monolayer of liposomes is clearly demonstrated since the full angular SPR spectrum was predicted by modeling and the conditions for the validity of the optical model were satisfied.

In general, the SPR curve produced by the MP-SPR provides averaged information from the entire SPR chip surface. There are factors that can influence the thicknesses and refractive indexes of the layers such as gaps in the layers, inhomogeneous coverage or multilayer formation.[42] In our case, the small difference of theoretical thickness and refractive index of the different layers in comparison with the calculated values can be related to the gold surface roughness or defect area of grafted biomolecules.

Mono-Rhamnolipid interactions with immobilized biotinylated liposomes. The MP-SPR technique allows direct measurement of interactions in real time and without labeling. Figure 5 shows the full sensorgram for successive injections of mono-RLs at different concentrations. First, the injection of 1×10^{14} lipo mL^{-1} of liposomes on the streptavidin layer yielded a +1.58 ° variation of the θ_{SPR}. After stabilization of the signal in 0.15M NaCl, state III of the sensorgram corresponded

to the liposome-functionalized SPR chip. Then, the injection of different concentrations of mono-RLs caused definite variations of the SPR signal, showing that RLs interacted with the liposome layer, as described in the literature. [26, 43-44] A progressive destabilization of the liposome layer was observed upon successive injections of mono-RLs. The θ_{SPR} decreased and then stabilized when the lipid layer reached a second state (state IV). At the end of the experiment, a final state of the surface was reached upon the injection of Triton X-100 (1 %) followed by stabilization under the electrolyte flow (state V). The signal variation as a function of the RL concentration was reproducible from one experiment to another as is shown in the two sensorgrams presented in Figure 5 and Figure S3 (see Supporting Information). Figure S4 (see Supporting Information) exhibits the corresponding full-angle SPR scans and calculated fits from LayerSolver modeling associated with the III, IV and V states, respectively.

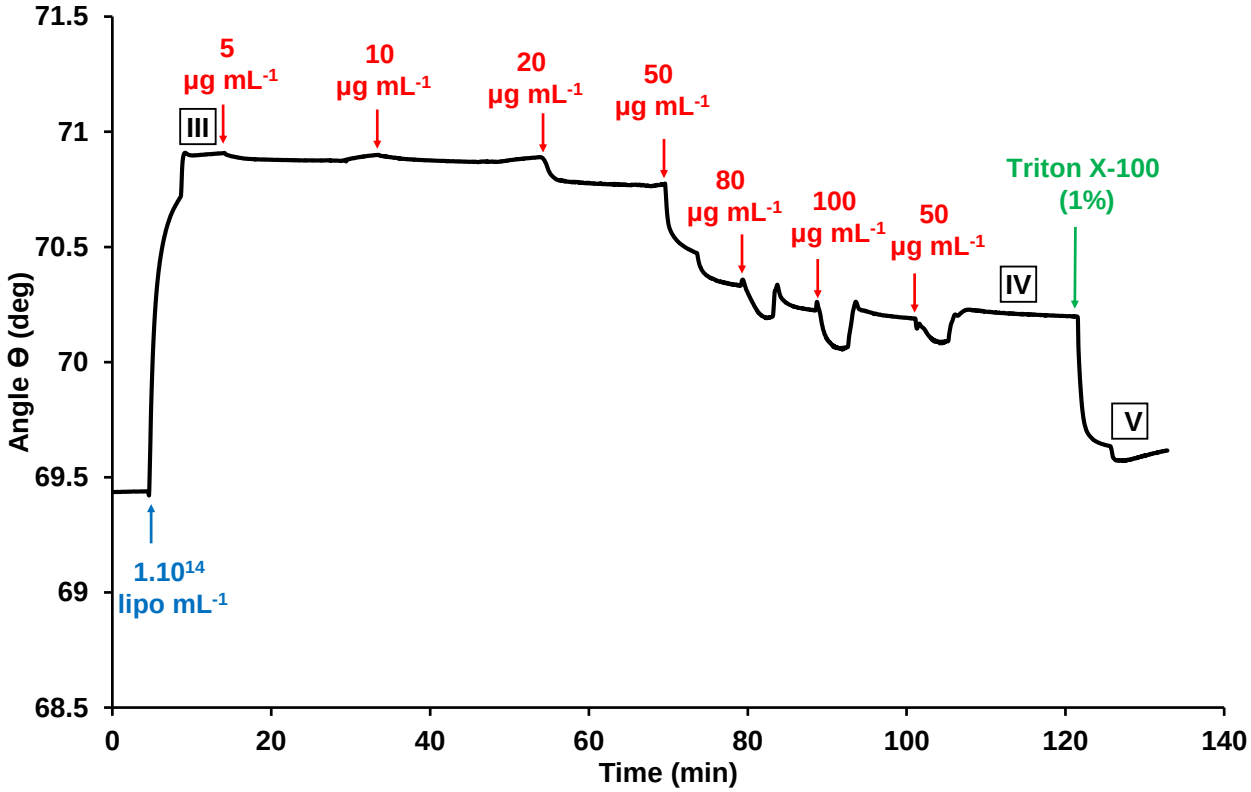

Figure 5. Sensorgram of the SPR angle versus time, measured at a wavelength of 670 nm, during the interaction of mono-RLs with liposomes.

Considering the sensorgram presented in Figure 5, it is worth noting that the mono-RLs were immediately captured by the lipid layer of the liposomes and signal variation resulted from the change of thickness and/or refractive index of the layer after adsorption. The variations of the SPR signal revealed different phenomena on the liposome layer depending on the concentration of mono-RLs. We can differentiate three domains for which the interactions of mono-RLs with the model membrane seem to follow different mechanisms. From 2 to 20 µg mL^{-1} mono-RLs, the sensorgram showed a progressive decrease of the SPR signal upon injection. We believe that RLs intercalate in the phospholipid layer without destructuring the liposomes. This interaction probably follows an equilibrium between free RLs in solution and molecules integrated into the lipid bilayer. This leads to a drop in SPR signal related to the concentration of RLs. Then, the SPR signal significantly dropped upon 50 µg mL^{-1} mono-RL injection. A structural change in the liposome layer was hypothesized at this concentration. The 50 µg mL^{-1} concentration is close to the critical micellar concentration (CMC) for mono-RLs, as the value reported in the literature is 56.3 µg mL^{-1} (~110 µM). [45-47] At 50 µg mL^{-1} concentration, the mono-RLs plunged into the double lipid layer of liposomes, thereby destabilizing their structure as closed bilayers. Opening the liposomes obviously should cause the formation of an adsorbed bilayer at the surface of the chip. The excess of phospholipids was presumably washed off by the mono-RL solution by means of solubilization inside the micelles. This phenomenon was irreversible. Then, the injections of higher concentrations of mono-RLs (80 µg mL^{-1} and 100 µg mL^{-1}) produced another different behavior. A drop in the angular shift of the SPR peak was observed, followed by a rise of the signal back to the original value when switching to NaCl solution. A reversible adsorption of mono-RLs onto the

phospholipid bilayer was taking place, even after injection of the last concentration (50 µg mL^{-1}). This phenomenon could be explained by the property of RLs to induce a phase dissociation and partitioning of the phospholipid bilayer, as described by Herzog *et al.* [26] These authors showed by AFM and confocal fluorescence microscopy that rhamnolipids were able to cause a phase separation of the phospholipid bilayer into liquid-ordered (lo) and liquid-disordered (ld) phases. The AFM measurement showed a thinner bilayer thickness of the ld phase compared to the lo phase. This mechanism was reversible, depending on the concentration of each constituent in the medium. Thus, in our case, the phospholipid organization as a bilayer seems to reform on the SPR chip surface when the eluting solvent changed from the mono-RL solution back to the NaCl solution, which caused the release of a large amount of mono-RLs in solution. This mechanism could explain the drop, and then the rise back up, of the signal observed during the study.

Figure 6 shows the SPR angular shifts ($\Delta\theta$) with respect to the streptavidin layer following the successive injection of mono-RLs and then Triton X-100 (1 %) on the SPR gold chip. It is interesting to note that when the mono-RLs bound to lipid vesicles, the SPR angular shifts ($\Delta\theta$) decreased (red bars), then dropped down further after the injection of Triton X-100 (1 %) (green bar). This behavior is also shown in Figure S4 (Supporting Information) since the θ_{SPR} corresponding to the liposome layer (state III) shifted to the left upon mono-RL action on the biomimetic surface. This phenomenon takes place when the mass or thickness of the layer changes. In our case, the shift towards the minimum SPR angles up to state IV and then state V is equivalent to a mass decrease of the molecules coating the SPR gold chip due to a high degree of lipid vesicle lysis.

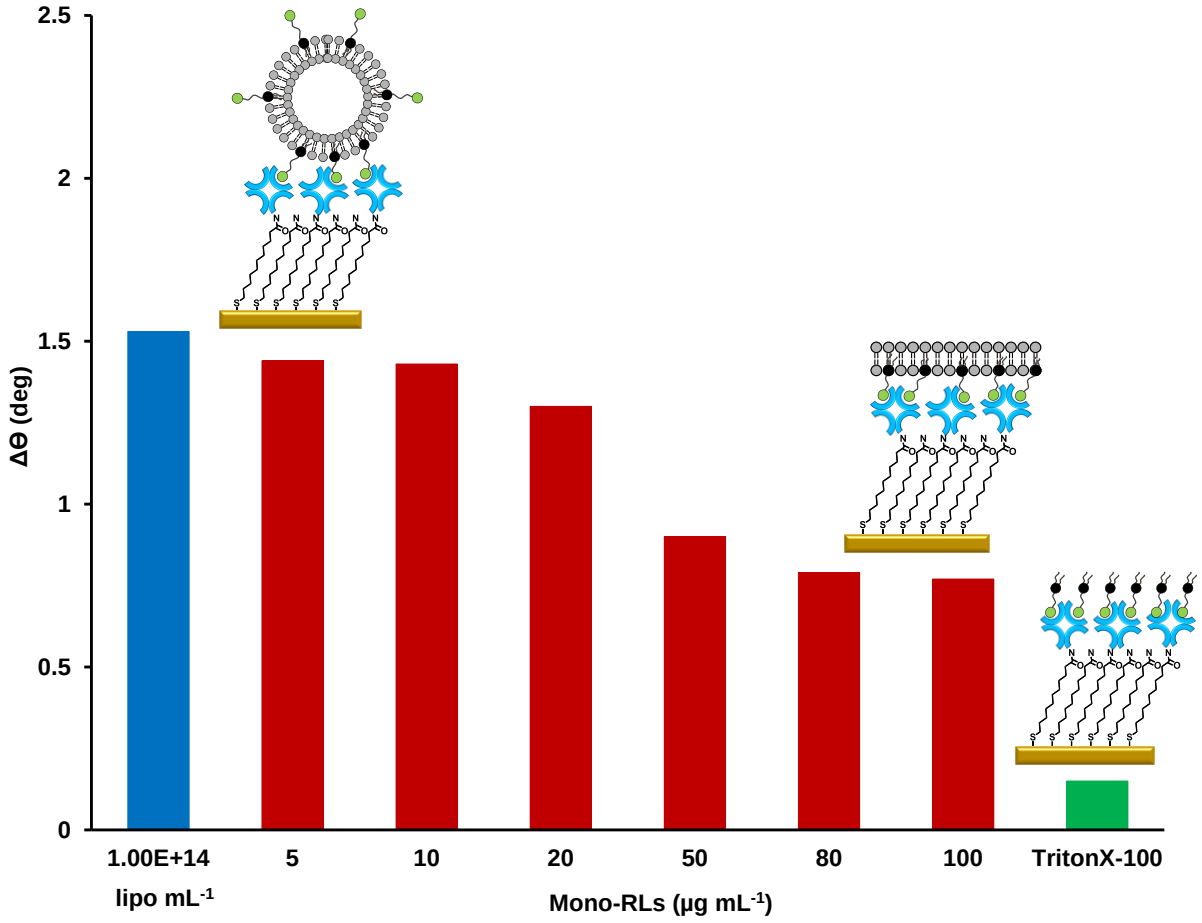

Figure 6. Sketches of the morphology changes of the liposome layer associated with the angular shifts of the SPR resonance peak following injections of mono-RLs and Triton X-100 (1 %) onto the liposome layer.

Mono-RLs induce a strong destructuration of the liposomes, which requires the rupture of the vesicle membrane to form a lipid bilayer laterally connected to the surface of the gold chip. After each injection of RLs, a 4-minute washing step of the SPR chip with 0.15M NaCl is performed for signal stabilization. The average thicknesses (*d*) and refractive indexes (*n*) of layers at the three

stages (III, IV and V) indicated in Figure 5 are calculated after signal stabilization in 0.15M NaCl (Table 3).

Table 3: Thickness (*d*) and refractive index (n_{670}) obtained from the SPR analysis in 0.15 M NaCl, for the liposome layer deposited on streptavidin and for the resulting lipid layers after injection of mono-RLs and Triton X-100 (1 %). The calculated values represent the average (± standard deviation) of three independent measurements.

Layer	*d* (nm)	n_{670}
Liposomes (III)	79.61 ± 6.74	1.35270 ± 0.00122
Lipid bilayer (IV)	5.60 ± 0.01	1.44941 ± 0.00042
Lipid monolayer (V)	2.30 ± 0.43	1.41931 ± 0.00033

According to results shown in Table 3, layer IV has a thickness around 5.6 nm, which is very thin compared to the initial liposome layer (III). This thickness calculated by modeling the SPR curve corresponds to the layer that remains attached to the SPR gold chip after the interaction with mono-RLs. This value is comparable to the theoretical thickness of a lipid bilayer containing both HSPC and DSPC-PEG lipids (~6 nm). Our results can also be compared to data from the literature on the thickness and refractive index values calculated for lipid bilayers with various types of lipids; POPC (d = 4.976 nm, n = 1.4788), DOPC (d = 3.992 nm, n = 1.456) and DMPC (d = 4.980 nm, n = 1.4810), [35] and HSPC (d ~ 6 nm, n = 1.404).[8]

The injection of Triton X-100 (1 %) on layer IV left a thin layer V on the streptavidin whose calculated thickness was 2.3 nm. According to the literatures,[8, 13, 40] this value is comparable to the

thickness of a lipid monolayer. This layer corresponds to biotinylated lipids (DSPE-PEG) that remained attached to streptavidin due to the high strength of the biotin-streptavidin interaction.

Thanks to the theoretical modeling and calculation of the optical parameters of the layers, we were able to estimate the quantity of lipids grafted on the SPR gold chip after the interaction of the liposomes with mono-RLs and Triton X-100 (1 %). This study was achieved in order to better understand the effect of the lytic mode of action of the mono-RLs against the lipids contained in the liposome layer immobilized on streptavidin. The surface mass densities of lipids bound to the surface of the SPR gold chip were calculated for the three layers (III, IV and V) using equation (3) and the theoretical values obtained in Table 3. Hence, the surface mass densities of lipids were Γ(III) ~ 1226 ng cm^{-2} for the immobilized liposome layer, then Γ(IV) ~ 490 ng cm^{-2} for the lipid bilayer, and finally Γ(V) ~ 150 ng cm^{-2} for the amount of lipids remaining on the streptavidin layer.

The surface mass density of lipids calculated for state III corresponds to a monolayer of liposomes as described in the literature (surface mass density Γ = 1557.64 ng cm^{-2} for liposomes with a diameter of 86.63 nm).[23] In our case, this mass corresponds to 1.32 ×10^{10} liposomes per cm^{-2}. This value can be compared to the theoretical maximum number of spheres of 80 nm diameter deposited on a surface as the geometric prediction of a densely packed monolayer of spheres (1.8×10^{10} nanosphere cm^{-2}) and calculated with equation S2. The lipid mass calculated in our case confirms that we have developed a dense layer of liposomes on the sensor surface. The slightly lower coverage rate compared to the theoretical value can be explained by the fact that deposition in aqueous phase is strongly impacted by the hydrodynamic diameter and surface nature (negative charge and presence of biotin arms) of the lipidic vesicles.

The lipid mass observed after the interaction with mono-RLs (state IV) is expected to be a single lipid bilayer, as the calculated mass is comparable to values from previously published measurements.[36, 48]

The present SPR device can be used as a sensitive biosensor for mono-RL detection because the interaction with a layer of immobilized liposomes was highly dependent on the concentration. Increasing the mono-RL concentration up to 50 μg mL^{-1} led to a decrease of the θ_{SPR}. Starting from the minimum angular value of the liposome layer, a $\Delta\theta_c$ increase from 0.015 ° to 0.47 ° (absolute values) was observed after injection of mono-RLs from 2 μg mL^{-1} to 50 μg mL^{-1} respectively. The $\Delta\theta_c$ shift indicates that the liposome-coated SPR chip detects mono-RLs even at low concentrations. Based on these results, we experimentally determined the mono-RL detection limit at 2 μg mL^{-1} (~3 μM). The detection threshold was established as three times the standard deviation of the SPR angle measurement recorded from three independent injections of NaCl 0.15 M solution ($\Delta\theta_c$ threshold : 0.005°). The sensitivity range of the method corresponds well to the concentrations of Rhamnolipids that have been detected in sputum of patients with acute *P. Aeruginosa* infection (~1-10 μg mL^{-1}). [49] The sensorgram also shows that the SPR chip was able to respond immediately and continuously, indicating the ability of liposomes to monitor the presence of mono-RLs in real time.

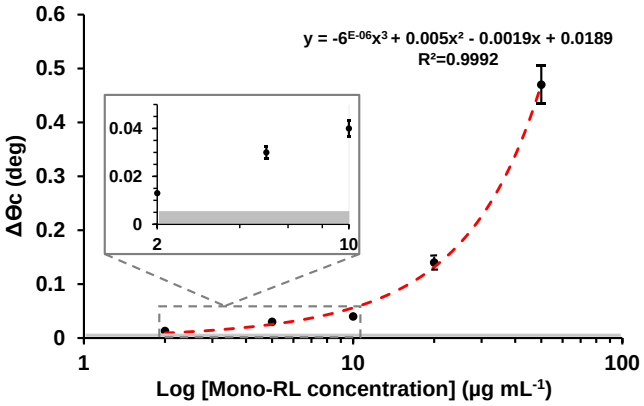

Figure 7. Cumulated $\Delta\Theta_c$ (absolute values) versus different concentrations of mono-RLs onto the liposome-coated SPR chip (average values of two experiments).

Our SPR chip showed good analytical performance in terms of sensitivity compared to previous studies describing other methods for RL detection. Indeed, the liposome-based fluorescence assay developed by Jenkins' group was able to detect certain toxins such as RLs with a LoD of 10 µg mL^{-1}.[44] The fluorescent signal of the assay showed a non-linear response versus RL concentration from 10 µg mL^{-1} to 80 µg mL^{-1} in solution. Jenkins' group also proved that RLs were detected in real samples of *P. aeruginosa* strains isolated from either chronic or acute infections. [50] This liposome-based fluorescence assay was recently validated for the detection of toxins associated with several bacteria including *P. aeruginosa*, *Staphylococcus aureus*, *Candida albicans*, *Candida auris*, and *Enterococcus faecalis* species in wound samples. A good correlation was demonstrated between the fluorescent sensor switch-on and early-stage wound infection. [51] A high performance liquid chromatography coupled to a charged-aerosol detection (HPLC-CAD) method was also developed by Behrens *et al*. with a LoD for RLs of 1 µg mL^{-1}.[52] One can note that the LoD reached by this highly sensitive technique is close to that of the proposed MP-SPR technique in this work. Thus, our strategy based on the use of a biomimetic membrane coupled to a measurement by SPR

appears to be a robust and sensitive analytical approach for the easy detection of biosurfactants such as RLs.

CONCLUSION

A biomimetic surface formed of liposomes grafted onto a gold substrate was developed for the study of interactions with biosurfactants by the MP-SPR method. First, we optimized the liposome anchoring on the SPR gold chip surface *via* a biotin/streptavidin binding strategy in order to investigate their interactions with RLs. The SPR signal variation clearly illustrated the binding affinity and the formation of a very stable liposome layer on the streptavidin functionalized surface, with high coverage. Monitoring the angular shifts proved to be reproducible from one experiment to another. We demonstrated the capacity of the MP-SPR technique to characterize the different states of the liposome architecture, i.e. from a monolayer of lipid vesicles to a single lipid bilayer induced by the interaction with mono-RLs and then a lipid monolayer resulting from Triton X-100 (1 %) treatment. This assumption was proven theoretically by calculating the thickness (d) and refractive index ($\tilde{n}$) of our multilayer system via the SPR Navi LayerSolver software. The modeling of the experimental data was successful and the small difference observed was mainly attributed to gold surface roughness. In addition, we were able to calculate the surface mass density (Γ) of the lipid layers on the SPR chip surface after the interaction of liposomes with mono-RLs and Triton X-100 (1 %) successively. The MP-SPR characterization method is generic and can be adapted to any multilayer system undergoing morphological and quantitative transformations during the adsorption of biomolecules on their surfaces. This analytical tool proved its high sensitivity for the detection of RLs, with a detection limit of 2 µg mL^{-1}. Further studies are still needed to validate our method in real samples. On this point, it is important to note that although the test is probably

not specific for the detection of rhamnolipids from *P. aeruginosa*, it may be of interest for the sensitive detection of bacterial toxins at the early stage of an infection. In summary, the use of MP-SPR and layer-by-layer modeling is a powerful combination to identify and quantify biomolecular layers deposited on a solid surface. This could open interesting perspectives to understand and study other mechanisms of interaction and transitions in membranes induced by biologically relevant processes such as membrane-interacting peptides or membrane active drugs.

ACKNOWLEDGEMENTS

The authors would like to thank the Tunisian government for financial support of Meryem Belkilani's PhD thesis and the Institut de Chimie de Lyon (ICL) for funding support. The authors also acknowledge Pierre-Yves Dugas, C2P2 Laboratory, UMR CNRS 5128, Lyon 1 University, for the Cryo-TEM characterization of liposomes.

SUPPORTING INFORMATION

Liposome concentration calculation (equation S1), theoretical maximum number of nanospheres deposited on a surface (equation S2), effect of Triton X-100 (1 %) detergent on the SPR response (Figure S1), SPR full angle scans at the different steps of the SPR gold chip functionalization (Figure S2), compiled modeling results (Table S1), sensorgram of the mono-RL/liposome interaction (Figure S3), measured and modeled SPR full angle scans of the liposome layer at 670 nm (Figure S4).

ABBREVIATIONS

Mono-RL, mono-Rhamnolipid; MP-SPR, Multi-parametric surface plasmon resonance; MUA, 11-mercaptoundecanoic acid; DLS, Dynamic Light Scattering; *PdI*, polydispersity index; Cryo-TEM, Cryo transmission electron microscopy; SAM, self-assembled monolayers; *SD*, standard deviation; θ_{SPR}, SPR angular peak minimum.

REFERENCES

(1) Zulianello, L.; Canard, C.; Köhler, T.; Caille, D.; Lacroix, J.-S.; Meda, P. Rhamnolipids are virulence factors that promote early infiltration of primary human airway epithelia by Pseudomonas aeruginosa. *Infect. Immun.* **2006,** *74* (6), 3134-3147.

(2) Santos, D. K. F.; Rufino, R. D.; Luna, J. M.; Santos, V. A.; Sarubbo, L. A. Biosurfactants: multifunctional biomolecules of the 21st century. *Int. J. Mol. Sci.* **2016,** *17* (3), 401.

(3) Lebègue, E.; Farre, C.; Jose, C.; Saulnier, J.; Lagarde, F.; Chevalier, Y.; Chaix, C.; Jaffrezic-Renault, N. Responsive polydiacetylene vesicles for biosensing microorganisms. *Sensors* **2018,** *18* (2), 599.

(4) Lebegue, E.; Farre, C.; Jose, C.; Saulnier, J.; Lagarde, F.; Chevalier, Y.; Chaix, C.; Jaffrezic-Renault, N. Biomimetic vesicles for electrochemical sensing. *Curr. Opin. Electrochem.* **2018,** *12*, 101-106.

(5) Aranda, F. J.; Espuny, M. J.; Marqués, A.; Teruel, J. A.; Manresa, Á.; Ortiz, A. Thermodynamics of the interaction of a dirhamnolipid biosurfactant secreted by Pseudomonas aeruginosa with phospholipid membranes. *Langmuir* **2007,** *23* (5), 2700-2705.

(6) Monnier, N.; Furlan, A. L.; Buchoux, S.; Deleu, M.; Dauchez, M.; Rippa, S.; Sarazin, C. Exploring the dual interaction of natural rhamnolipids with plant and fungal biomimetic plasma membranes through biophysical studies. *Int. J. Mol. Sci.* **2019,** *20* (5), 1009.

(7) Chen, M.; Penfold, J.; Thomas, R.; Smyth, T.; Perfumo, A.; Marchant, R.; Banat, I.; Stevenson, P.; Parry, A.; Tucker, I. Solution self-assembly and adsorption at the air− water interface of the monorhamnose and dirhamnose rhamnolipids and their mixtures. *Langmuir* **2010,** *26* (23), 18281-18292.

(8) Granqvist, N.; Liang, H.; Laurila, T.; Sadowski, J.; Yliperttula, M.; Viitala, T. Characterizing ultrathin and thick organic layers by surface plasmon resonance three-wavelength and waveguide mode analysis. *Langmuir* **2013,** *29* (27), 8561-8571.

(9) Kari, O. K.; Rojalin, T.; Salmaso, S.; Barattin, M.; Jarva, H.; Meri, S.; Yliperttula, M.; Viitala, T.; Urtti, A. Multi-parametric surface plasmon resonance platform for studying liposome-serum interactions and protein corona formation. *Drug Deliv. Transl. Res.* **2017,** *7* (2), 228-240.

(10) Plant, A. L.; Brighamburke, M.; Petrella, E. C.; Oshannessy, D. J. Phospholipid/alkanethiol bilayers for cell-surface receptor studies by surface plasmon resonance. *Anal. Biochem.***1995,** *226* (2), 342-348.

(11) Keller, C.; Glasmästar, K.; Zhdanov, V.; Kasemo, B. Formation of supported membranes from vesicles. *Phys. Rev. Lett.* **2000,** *84* (23), 5443.

(12) Reimhult, E.; Zäch, M.; Höök, F.; Kasemo, B. A multitechnique study of liposome adsorption on Au and lipid bilayer formation on SiO2. *Langmuir* **2006,** *22* (7), 3313-3319.

(13) Granqvist, N.; Yliperttula, M.; Välimäki, S.; Pulkkinen, P.; Tenhu, H.; Viitala, T. Control of the morphology of lipid layers by substrate surface chemistry. *Langmuir* **2014,** *30* (10), 2799-2809.

(14) Fenzl, C.; Hirsch, T.; Baeumner, A. J. Liposomes with high refractive index encapsulants as tunable signal amplification tools in surface plasmon resonance spectroscopy. *Anal. Chem.* **2015,** *87* (21), 11157-11163.

(15) Fenzl, C.; Genslein, C.; Domonkos, C.; Edwards, K.; Hirsch, T.; Baeumner, A. Investigating non-specific binding to chemically engineered sensor surfaces using liposomes as models. *Analyst* **2016,** *141* (18), 5265-5273.
(16) Sacconi, A.; Tadini-Buoninsegni, F.; Tiribilli, B.; Margheri, G. A Comparative Study of Phosphatidylcholine versus Phosphatidylserine-Based Solid Supported Membranes for the Preparation of Liposome-Rich Interfaces. *Langmuir* **2018,** *34* (40), 12183-12190.
(17) Xiang, Y.; Kiseleva, R.; Reukov, V.; Mulligan, J.; Atkinson, C.; Schlosser, R.; Vertegel, A. Relationship between targeting efficacy of liposomes and the dosage of targeting antibody using surface plasmon resonance. *Langmuir* **2015,** *31* (44), 12177-12186.
(18) Parkkila, P.; Viitala, T. Partitioning of Catechol Derivatives in Lipid Membranes: Implications for Substrate Specificity to Catechol-O-methyltransferase. *ACS Chem. Neurosci.* **2020,** *11* (6), 969-978.
(19) Baird, C. L.; Courtenay, E. S.; Myszka, D. G. Surface plasmon resonance characterization of drug/liposome interactions. *Anal. Biochem.* **2002,** *310* (1), 93-99.
(20) Mozsolits, H.; Aguilar, M. I. Surface plasmon resonance spectroscopy: an emerging tool for the study of peptide–membrane interactions. *Peptide Science: Original Research on Biomolecules* **2002,** *66* (1), 3-18.
(21) Skyttner, C.; Enander, K.; Aronsson, C.; Aili, D. Tuning Liposome Membrane Permeability by Competitive Coiled Coil Heterodimerization and Heterodimer Exchange. *Langmuir* **2018,** *34* (22), 6529-6537.
(22) Beseničar, M.; Maček, P.; Lakey, J. H.; Anderluh, G. Surface plasmon resonance in protein–membrane interactions. *Chem. Phys. Lipids* **2006,** *141* (1-2), 169-178.
(23) Kari, O. K.; Ndika, J.; Parkkila, P.; Louna, A.; Lajunen, T.; Puustinen, A.; Viitala, T.; Alenius, H.; Urtti, A. In situ analysis of liposome hard and soft protein corona structure and composition in a single label-free workflow. *Nanoscale* **2020,** *12* (3), 1728-1741.
(24) Coutable, A. l.; Thibault, C.; Chalmeau, J. r. m.; François, J. M.; Vieu, C.; Noireaux, V.; Trévisiol, E. Preparation of tethered-lipid bilayers on gold surfaces for the incorporation of integral membrane proteins synthesized by cell-free expression. *Langmuir* **2014,** *30* (11), 3132-3141.
(25) Palacios-Ortega, J.; García-Linares, S.; Åstrand, M.; Al Sazzad, M. A.; Gavilanes, J. G.; Martínez-del-Pozo, A. l.; Slotte, J. P. Regulation of sticholysin II-induced pore formation by lipid bilayer composition, phase state, and interfacial properties. *Langmuir* **2016,** *32* (14), 3476-3484.
(26) Herzog, M.; Tiso, T.; Blank, L. M.; Winter, R. Interaction of rhamnolipids with model biomembranes of varying complexity. *Biochim. et Biophys. Acta (BBA)-Biomembr.* **2020**, 183431.
(27) Zhao, Y.; Du, D.; Lin, Y. Glucose encapsulating liposome for signal amplification for quantitative detection of biomarkers with glucometer readout. *Biosens. Bioelectron.* **2015,** *72*, 348-354.
(28) Baccar, H.; Mejri, M.; Hafaiedh, I.; Ktari, T.; Aouni, M.; Abdelghani, A. Surface plasmon resonance immunosensor for bacteria detection. *Talanta* **2010,** *82* (2), 810-814.
(29) Albers, W. M.; Vikholm-Lundin, I. Surface plasmon resonance on nanoscale organic films. In *Nano-Bio-Sensing*; Springer: 2011, pp 83-125.
(30) Parkkila, P.; Elderdfi, M.; Bunker, A.; Viitala, T. Biophysical characterization of supported lipid bilayers using parallel dual-wavelength surface plasmon resonance and quartz crystal microbalance measurements. *Langmuir* **2018,** *34* (27), 8081-8091.

(31) Peterlinz, K.; Georgiadis, R. Two-color approach for determination of thickness and dielectric constant of thin films using surface plasmon resonance spectroscopy. *Opt. Commun.* **1996,** *130* (4-6), 260-266.
(32) Zhou, M.; Otomo, A.; Yokoyama, S.; Mashiko, S. Estimation of organic molecular film structures using surface–plasmon resonance spectroscopy. *Thin Solid Films* **2001,** *393* (1-2), 114-118.
(33) Viitala, T.; Granqvist, N.; Hallila, S.; Raviña, M.; Yliperttula, M. Elucidating the signal responses of multi-parametric surface plasmon resonance living cell sensing: a comparison between optical modeling and drug–MDCKII cell interaction measurements. *PloS one* **2013,** *8* (8), e72192.
(34) Chattoraj, D. K.; Birdi, K. S. *Adsorption and the Gibbs surface excess*, 1st ed.; Springer: Boston, 1984.
(35) Mashaghi, A.; Swann, M.; Popplewell, J.; Textor, M.; Reimhult, E. Optical anisotropy of supported lipid structures probed by waveguide spectroscopy and its application to study of supported lipid bilayer formation kinetics. *Anal. Chem.* **2008,** *80* (10), 3666-3676.
(36) Ye, Q.; Konradi, R.; Textor, M.; Reimhult, E. Liposomes tethered to omega-functional PEG brushes and induced formation of PEG brush supported planar lipid bilayers. *Langmuir* **2009,** *25* (23), 13534-13539.
(37) Haes, A. J.; Van Duyne, R. P. A nanoscale optical biosensor: sensitivity and selectivity of an approach based on the localized surface plasmon resonance spectroscopy of triangular silver nanoparticles. *J. Am. Chem. Soc.* **2002,** *124* (35), 10596-10604.
(38) Baba, A.; Taranekar, P.; Ponnapati, R. R.; Knoll, W.; Advincula, R. C. Electrochemical surface plasmon resonance and waveguide-enhanced glucose biosensing with N-alkylaminated polypyrrole/glucose oxidase multilayers. *ACS Appl. Mater. Interfaces* **2010,** *2* (8), 2347-2354.
(39) Damos, F. S.; Luz, R. C.; Kubota, L. T. Determination of thickness, dielectric constant of thiol films, and kinetics of adsorption using surface plasmon resonance. *Langmuir* **2005,** *21* (2), 602-609.
(40) Schmidt, A.; Spinke, J.; Bayerl, T.; Sackmann, E.; Knoll, W. Streptavidin binding to biotinylated lipid layers on solid supports. A neutron reflection and surface plasmon optical study. *Biophys. J.* **1992,** *63* (5), 1385-1392.
(41) Dolci, M.; Bryche, J.-F.; Leuvrey, C.; Zafeiratos, S.; Gree, S.; Begin-Colin, S.; Barbillon, G.; Pichon, B. P. Robust clicked assembly based on iron oxide nanoparticles for a new type of SPR biosensor. *J. Mater. Chem. C* **2018,** *6* (34), 9102-9110.
(42) Hall, D. Kinetic models describing biomolecular interactions at surfaces. In *Handbook of Surface Plasmon Resonance*; Royal Society of Chemistry Cambridge: 2008; pp 81-122.
(43) Moussa, Z.; Chebl, M.; Patra, D. Interaction of curcumin with 1, 2-dioctadecanoyl-sn-glycero-3-phosphocholine liposomes: Intercalation of rhamnolipids enhances membrane fluidity, permeability and stability of drug molecule. *Colloids Surf. B* **2017,** *149*, 30-37.
(44) Thet, N. T.; Jamieson, W. D.; Laabei, M.; Mercer-Chalmers, J. D.; Jenkins, A. T. A. Photopolymerization of polydiacetylene in hybrid liposomes: effect of polymerization on stability and response to pathogenic bacterial toxins. *J. Phys. Chem. B* **2014,** *118* (20), 5418-5427.
(45) Guo, Y.-P.; Hu, Y.-Y. Solubilization of moderately hydrophobic 17α-ethinylestradiol by mono-and di-rhamnolipid solutions. *Colloids Surf. A Physicochem. Eng. Asp.* **2014,** *445*, 12-20.

(46) Guo, Y.-P.; Hu, Y.-Y.; Gu, R. R.; Lin, H. Characterization and micellization of rhamnolipidic fractions and crude extracts produced by Pseudomonas aeruginosa mutant MIG-N146. *J. Colloid Interface Sci.* **2009,** *331* (2), 356-363.
(47) Eismin, R. J.; Munusamy, E.; Kegel, L. L.; Hogan, D. E.; Maier, R. M.; Schwartz, S. D.; Pemberton, J. E. Evolution of aggregate structure in solutions of anionic monorhamnolipids: Experimental and computational Results. *Langmuir* **2017,** *33* (30), 7412-7424.
(48) Reimhult, E.; Larsson, C.; Kasemo, B.; Höök, F. Simultaneous surface plasmon resonance and quartz crystal microbalance with dissipation monitoring measurements of biomolecular adsorption events involving structural transformations and variations in coupled water. *Anal. Chem.* **2004,** *76* (24), 7211-7220.
(49) Kownatzki, R.; Tümmler, B.; Döring, G. Rhamnolipid of Pseudomonas aeruginosa in sputum of cystic fibrosis patients. *Lancet* **1987,** *1* (8540), 1026-1027.
(50) Laabei, M.; Jamieson, W. D.; Lewis, S. E.; Diggle, S. P.; Jenkins, A. T. A. A new assay for rhamnolipid detection—important virulence factors of Pseudomonas aeruginosa. *Appl. Microbiol. Biotechnol.* **2014,** *98* (16), 7199-7209.
(51) Thet, N. T.; Mercer-Chalmers, J.; Greenwood, R. J.; Young, A. E.; Coy, K.; Booth, S.; Sack, A.; Jenkins, A. T. SPaCE Swab: Point-of-Care Sensor for Simple and Rapid Detection of Acute Wound Infection. *ACS sensors* **2020,** *5* (8), 2652-2657.
(52) Behrens, B.; Baune, M.; Jungkeit, J.; Tiso, T.; Blank, L. M.; Hayen, H. High performance liquid chromatography-charged aerosol detection applying an inverse gradient for quantification of rhamnolipid biosurfactants. *J. Chromatogr. A* **2016,** *1455*, 125-132.

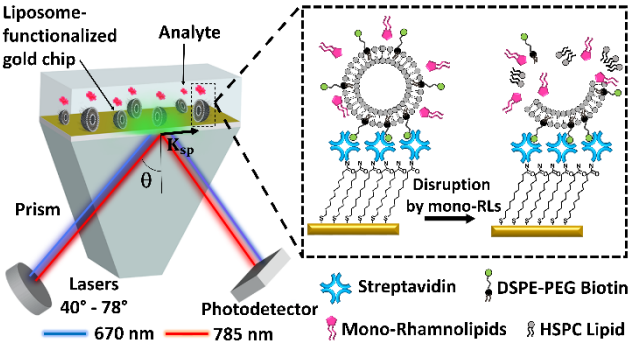
Liposome-
functionalized
gold chip
Analyte
K_{sp}
θ
Prism
Lasers
40° - 78°
Photodetector
670 nm
785 nm
Disruption
by mono-RLs
Streptavidin
DSPE-PEG Biotin
Mono-Rhamnolipids
HSPC Lipid